ACS Catalysis

Research Article

pubs.acs.org/acscatalysis

Formation of Active Sites on WO_3 Catalysts: A Density Functional Theory Study of Olefin Metathesis

Zhuo Cheng and Cynthia S. Lo*

Department of Energy, Environmental and Chemical Engineering, Washington University, Saint Louis, Missouri 63130, United States

ABSTRACT: Industrial demand for poly(propene) has spurred research on improved catalysts and mechanisms for propene production. Recently, tungsten trioxide (WO_3) was reported to exhibit high activity for the metathesis of ethene and 2-butene to form propene. The whole process is divided into two stages: (1) Initiation (i.e., formation of W-carbene active sites on WO_3 surfaces), and (2) Propagation (i.e., metathesis reaction on these active sites to yield propene). This study investigates the mechanism of W-carbene active site formation, using first-principles calculations based on density functional theory. For the WO_3 orthorhombic crystal, the (001) surface has been found to be the most stable, since it contains four chemically distinguishable types of surface atoms: 5-fold coordinate W_{5c}, 6-fold coordinate W_{6c}, 2-fold bridging oxygen O_{2c}, and singly coordinated oxygen O_{1c}. Because of the different energies of adsorption for ethene and 2-butene at these four types of active sites, we find that 2-butene forms W-carbene active sites more readily, with lower activation energies, than ethene, because of a combination of electrophilic and steric effects. These results reveal the relationship between WO_3 catalyst surface structure and activity for metathesis, which ultimately will guide the development of more active and selective catalysts for propene production.

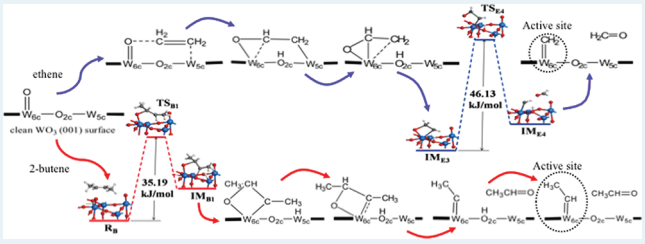

KEYWORDS: *DFT, tungsten oxide, metathesis, reaction pathway, active sites, ethene, 2-butene*

1. INTRODUCTION

In recent years, the metathesis of ethene ($H_2C{=}CH_2$) and 2-butene ($H_3C{-}CH{=}CH{-}CH_3$) to produce propene ($H_2C{=}CH{-}CH_3$) has attracted widespread interest because of increasing industrial demand for propene, which is an important chemical intermediate used as the building block for commodity chemicals ranging from plastic products to gasoline components. Traditionally, propene is produced by a steam cracking process that uses heat to produce a mixture of hydrocarbons from feedstocks such as ethane, propane, natural gas, or liquid petroleum products; these products then may be distilled to obtain propene.[1] Compared with the steam cracking method, however, metathesis reactions are promoted by catalysts and thus rely less on large sources of heat. Generally, heterogeneous catalysts containing Re, Mo, or W[2−6] are favored over homogeneous catalysts for this reaction because of their ease of separation, stability, and recyclability. Thus, olefin metathesis processes can be designed to be energy-efficient and cost-effective because they are solvent-free, generate little waste, require low catalyst loads, and operate with high yield.[7] Furthermore, the catalytic activity of these three transition metals is ascribed to the high reactivity of their unpaired d electrons, so that they can adopt multiple oxidation states to form active complexes and lower the activation energy of the metathesis reaction.[8]

As a metallic compound with W, tungsten trioxide WO_3 has received considerable attention for metathesis reactions, since it can maintain its stable structure within industrial reaction temperature ranges and can be easily deposited using physical or chemical approaches.[4,9−11] Several studies are highlighted here. Davazoglou et al.[12] claimed to obtain as equal metathesis activity with well dispersed low loading WO_3/SiO_2 catalysts as with catalysts of higher tungsten content indicating the importance of obtaining a well dispersed catalyst. Huang et al.[13,14] prepared a series of WO_3 catalysts by the thermal spread method and found that a proportional correlation between tetrahedral tungsten oxide species and metathesis activities. Liu et al.[15] showed that the formation of a surface (hydr)oxide layer on WO_3 is accelerated in the presence of a moist atmosphere, and discovered this shortens the calcination time required to produce highly active catalysts. Recently, Chaemchuen et al. obtained Raman, UV−vis, and H_2-TPR spectra suggesting that WO_3 catalysts calcined at 550 °C exhibit high activity for the metathesis of ethene and 2-butene to produce propene,[16] so the prospects for industrial-scale propene production via metathesis are extremely promising.

Hérisson and Chauvin were the first to postulate that metathesis can proceed rapidly at modest temperatures through a two step process: (1) Initiation to form metal-carbene active sites,[17−19] and (2) Propagation, including the [2 + 2] cycloaddition of alkene double bonds, at these metal-carbene active sites to form metallocyclobutane intermediates. A number of theoretical investigations[20−24] and experimental studies[25−28] have already confirmed the propagation steps in

Received: November 7, 2011
Revised: January 2, 2012
Published: January 7, 2012

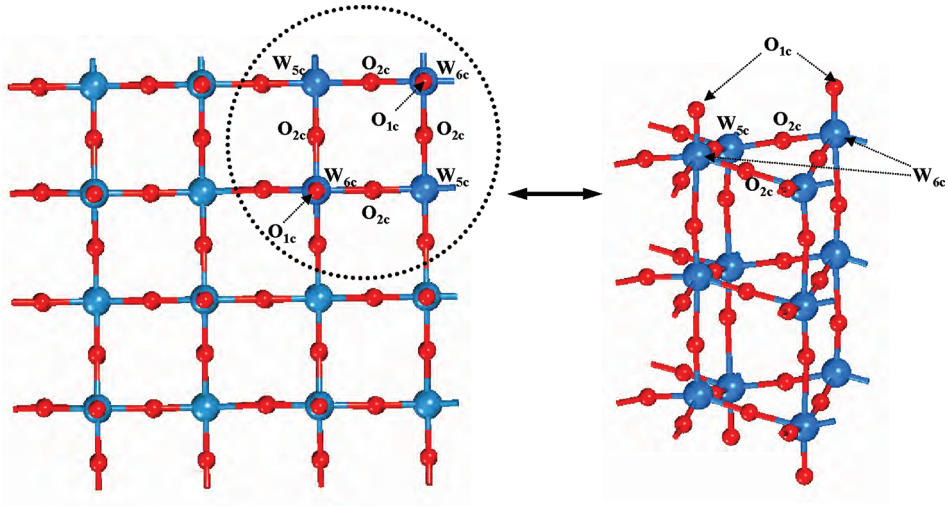

Figure 1. Geometry-optimized WO_3 (001) surface, showing the four chemically distinguishable types of surface atoms: (1) 5-fold coordinated tungsten W_{5c}, (2) 6-fold coordinated tungsten W_{6c}, (3) 2-fold bridging oxygen O_{2c}, and (4) singly coordinated oxygen O_{1c}.

the Hérisson−Chauvin mechanism. However, the process of forming the initial metal-carbene active sites is still not known, because of limitations in detecting the presence and molecular structure of the active sites with current spectroscopic techniques.[29] Thus, we focus here on the formation of these transition metal−alkylidene species that serve as active sites for further propagation steps.

In this work, we employ first-principles calculations based on density functional theory (DFT) to explore the energetics and kinetics of W-carbene active site formation on WO_3 surfaces. Theoretical/computational methods have been previously employed to study metal-catalyzed olefin reactions;[30−34] they provide fundamental insights that are relatively difficult to obtain experimentally (e.g., determination of the active sites, identification of possible reaction intermediates, nature of the transition states). We use a semi-infinite slab to model the catalyst structure and quantify its activity for olefin metathesis. The use of periodic models avoids the introduction of edge effects and allows for a more accurate description of surface relaxation. The stability of various surface terminations of WO_3 are calculated, and the correlation between the coordination of the tungsten and oxygen atoms in the oxide and the strength of gas molecule adsorption is determined. We thus show how the structure of the catalyst directly influences its activity for olefin metathesis. We also show the preferred pathway to form W-carbene active sites with calculated activation barriers.

2. METHODS

Tungsten trioxide (WO_3) exhibits perovskite-like structures with corner-sharing WO_6 octahedra. However, structural analyses of WO_3 have revealed considerable deviations from the ideal cubic perovskite type, with the majority of these distortions corresponding to antiferroelectric displacements of W atoms and mutual rotations of oxygen octahedra.[35] As in most perovskite-like substances, the magnitude of the distortion depends on the temperature of the sample.[36] WO_3 crystals melt at 1473 °C and undergo five phase transitions over the temperature range from 900 to −180 °C: tetragonal → orthorhombic → monoclinic → triclinic → monoclinic. At 550 °C, bulk WO_3 takes on the orthorhombic phase, and it is at this temperature that WO_3 catalysts have been shown to exhibit high activity for ethene and 2-butene metathesis.[16,37,38]While first-principles calculations are typically performed at 0 K, they have been used to model various phases of WO_3, including the orthorhombic phase.[39−41]

We thus use the orthorhombic phase for the WO_3 bulk. Its space group is *Pmnb*, with a = 7.341 Å, b = 7.570 Å, and c = 7.754 Å.[38] The deviation from the ideal perovskite structure is characterized by a zigzag motion of the W atomic positions in the b and c directions, as well as a tilt system with tilt angles around a.[42]

To build the surface slab models, the WO_3 bulk is cleaved along the (001) surface, which is chosen for consistency[41] with the majority of the published experimental studies on WO_3. The crystal is easily cleaved along the (001) surface since it is layered along this direction as a result of the antiferroelectric distortion of the W sublattice.[43,44] Thus, good quality single crystals of WO_3 (001) can be prepared by moderate heating in an oxygen-rich atmosphere[45−47] and characterized using scanning tunneling microscopy (STM), low energy electron diffraction (LEED), and photoelectron spectroscopy (UPS, XPS).[48,49]

Therefore, the WO_3 (001) surfaces were taken into account in the present study. The WO_3 (001) surface is modeled by a five-layer slab, with the bottom two atomic layers frozen in the bulk configuration and the top three atomic layers allowed to relax. A $p(2 \times 2)$ supercell is used to ensure that all adsorbates do not interact with their periodic images (i.e., separation by at least 10 Å). The WO_3 (001) surface thus consists of four chemically distinguishable types of surface atoms: (1) 5-fold coordinated tungsten W_{5c}, (2) 6-fold coordinated tungsten W_{6c}, (3) 2-fold bridging oxygen O_{2c}, and (4) singly coordinated oxygen O_{1c} (Figure 1).

All calculations are performed within the framework of DFT, using the Vienna Ab Initio Simulation Package (VASP 5.2)[50−52] and the generalized gradient approximation of Perdew, Burke, and Ernzerhof[53] to represent the exchange-correlation energy. The wave functions of the atomic cores are described using the Projector-Augmented Wave method (PAW) method,[54,55] which includes all plane waves with kinetic energies smaller than the chosen cutoff energy of 400 eV. This ensured an energy convergence within 1×10^{-5} eV, using the conjugate gradient method. We sample the Brillouin zone using a $6 \times 6 \times 6$ Monkhorst-Pack **k**-point mesh for the

dx.doi.org/10.1021/cs2005778 | ACS Catal. 2012, 2, 341−349

Scheme 1. Metathesis Reaction Pathways of Ethene and 2-Butene to Produce Propene[a]

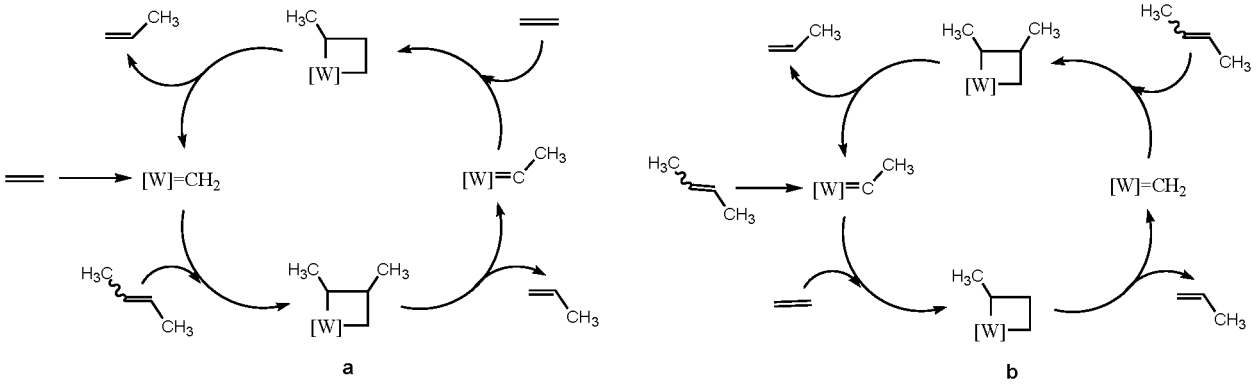

[a](a) Ethene reactant, (b) 2-butene reactant.

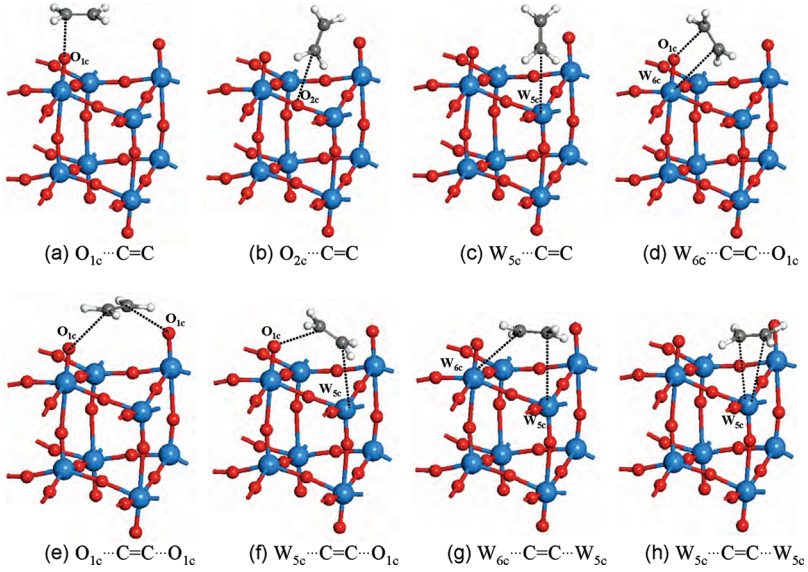

Figure 2. Optimized geometries, including bond lengths (Å), for ethene adsorbed to WO_3 (001).

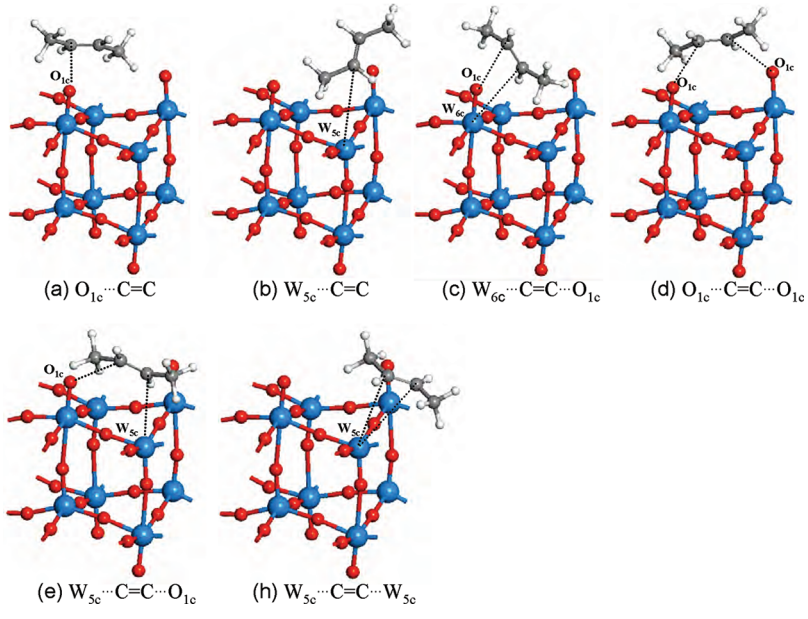

Figure 3. Optimized geometries, including bond lengths (Å), for 2-butene adsorbed to WO_3 (001).

dx.doi.org/10.1021/cs2005778 | ACS Catal. 2012, 2, 341−349

Table 1. Calculated Energies of Adsorption for Ethene and 2-Butene on WO_3 (001)

adsorption configuration	ethene E_{ads} (kJ/mol)	2-butene E_{ads} (kJ/mol)
	Monodentate	
O_{1c}···C=C	−22.39	−20.35
O_{2c}···C=C	−3.23	
W_{5c}···C=C	−21.40	−18.46
	Bidentate	
O_{1c}···C=C···O_{1c}	−8.01	−1.74
W_{5c}···C=C···O_{1c}	−26.73	−14.18
W_{6c}···C=C···O_{1c}	−15.15	−18.24
W_{5c}···C=C···W_{5c}	−24.31	−14.38
W_{6c}···C=C···W_{5c}	−23.83	

Scheme 2. Formation Pathway of Active Sites from Ethene and 2-Butene on WO_3 (001): (Left) Ethene Pathway, and (Right) 2-Butene Pathway

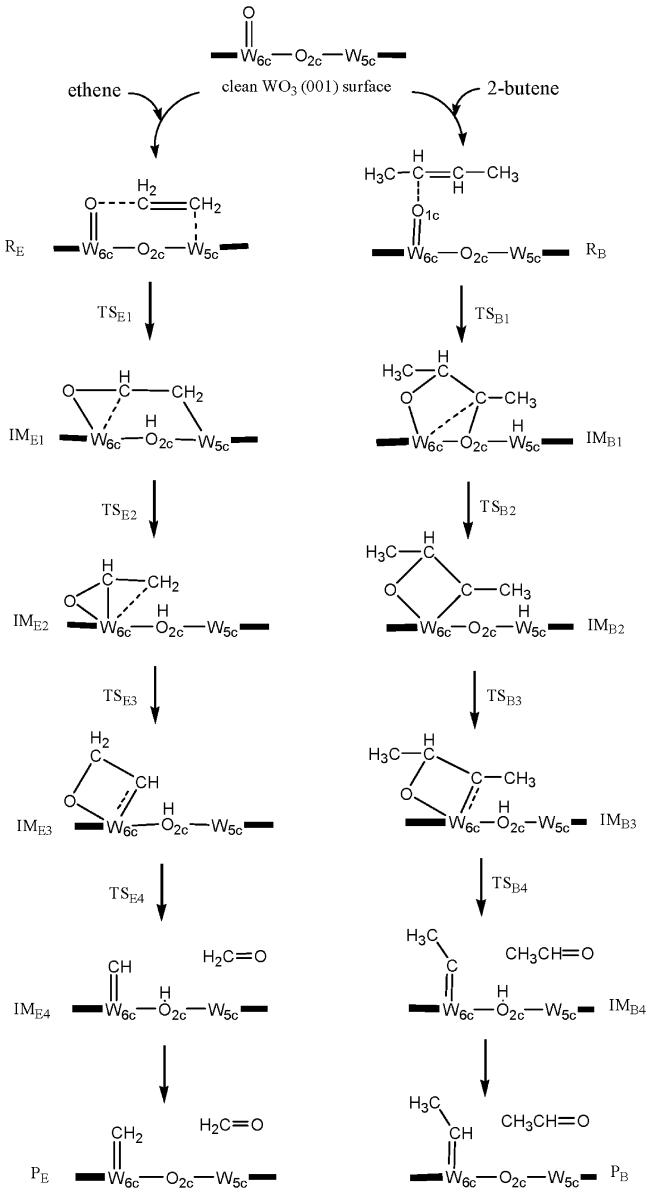

WO_3 bulk,[39] and a 6 × 6 × 1 **k**-point mesh for the WO_3 surface slab. We observed that spin-polarized calculations did not yield significant changes to the calculated energies compared to nonspin-polarized calculations.[56]

The energy of adsorption, E_{ads}, for the olefin molecules on the surface is defined as:

$$E_{ads} = E_{adsorbate+surface} - E_{surface} - E_{adsorbate} \quad (1)$$

where $E_{surface}$ is the total energy of the surface slab, $E_{adsorbate}$ is the total energy of the gas-phase adsorbate, and $E_{adsorbate+surface}$ is the total energy of the composite system. Since the calculations are performed at 0 K and fixed cell volume, the differences in Gibbs free energy should equal the differences in total energy. By this definition, a negative value of E_{ads} corresponds to an exothermic and spontaneous adsorption process. We also assume that the entropic contribution to the Gibbs free energy is negligible since the translational, vibrational, and rotational entropies of the gas-phase adsorbate should not change significantly upon adsorption. Thus, the change in Gibbs free energy with temperature for this system is likely to be small, since $((\partial G)/(\partial T))_P = -S$.

To locate saddle points and calculate the reaction pathway, we used the nudged elastic band (NEB) method;[57] this method is a "chain of states" method, where several intermediate states, or images, of the system are connected by springs to map out a reaction pathway between the initial and final states. By selecting an appropriate spring constant, we optimize the intermediate images by including only the parallel component of the spring force and the perpendicular component of the true force. We use four intermediate images for each NEB calculation and optimize these images to yield a minimum energy path. Because these paths are directed by force projection, the energy is not consistent with the force being optimized. Therefore, we choose the force-based quick-min optimizer to ensure that the NEB algorithm converges. The time step employed is 0.01 fs. Since we established that calculations at 0 K do not significantly change the Gibbs free energy, we anticipate that the calculated activation energy barriers and reaction pathway should be representative of the true reaction under industrial operating conditions.

3. RESULTS

3.1. Proposed Mechanism for Formation of W-Carbene Active Sites. As suggested by the Herisson–Chauvin mechanism, the initiating and propagating intermediates in olefin metathesis are metal-carbene species. These may be formed from either ethene or 2-butene in our reaction. The metathesis reaction proceeds with these two reactants, as shown in Scheme 1.

3.2. Adsorption of Ethene and 2-Butene on WO_3 (001). Ethene molecules can adsorb on the WO_3 (001) surface by single site adsorption (on the O site or W site) or two site adsorption (on the two O sites, two W sites, or one O and one W site). The possible adsorption configurations, after geometry optimization, are shown in Figures 2 and 3. The calculated energies of adsorption are listed in Table 1.

As shown in Table 1 for ethene adsorption, the two site adsorption configuration corresponding to W_{5c}···C=C···O_{1c} is the most energetically favorable, with E_{ads} = −26.73 kJ/mol. By contrast, the configuration corresponding to O_{1c}···C=C···O_{1c} is the least energetically favorable, with E_{ads} = −8.01 kJ/mol; the low energy of adsorption may be attributed to the large distance separating both O_{1c} sites ($r_{O_{1c}\cdots O_{1c}}$ = 5.455 Å), so that ethene cannot physically bond to both oxygen sites. Similarly,

dx.doi.org/10.1021/cs2005778 | ACS Catal. 2012, 2, 341–349

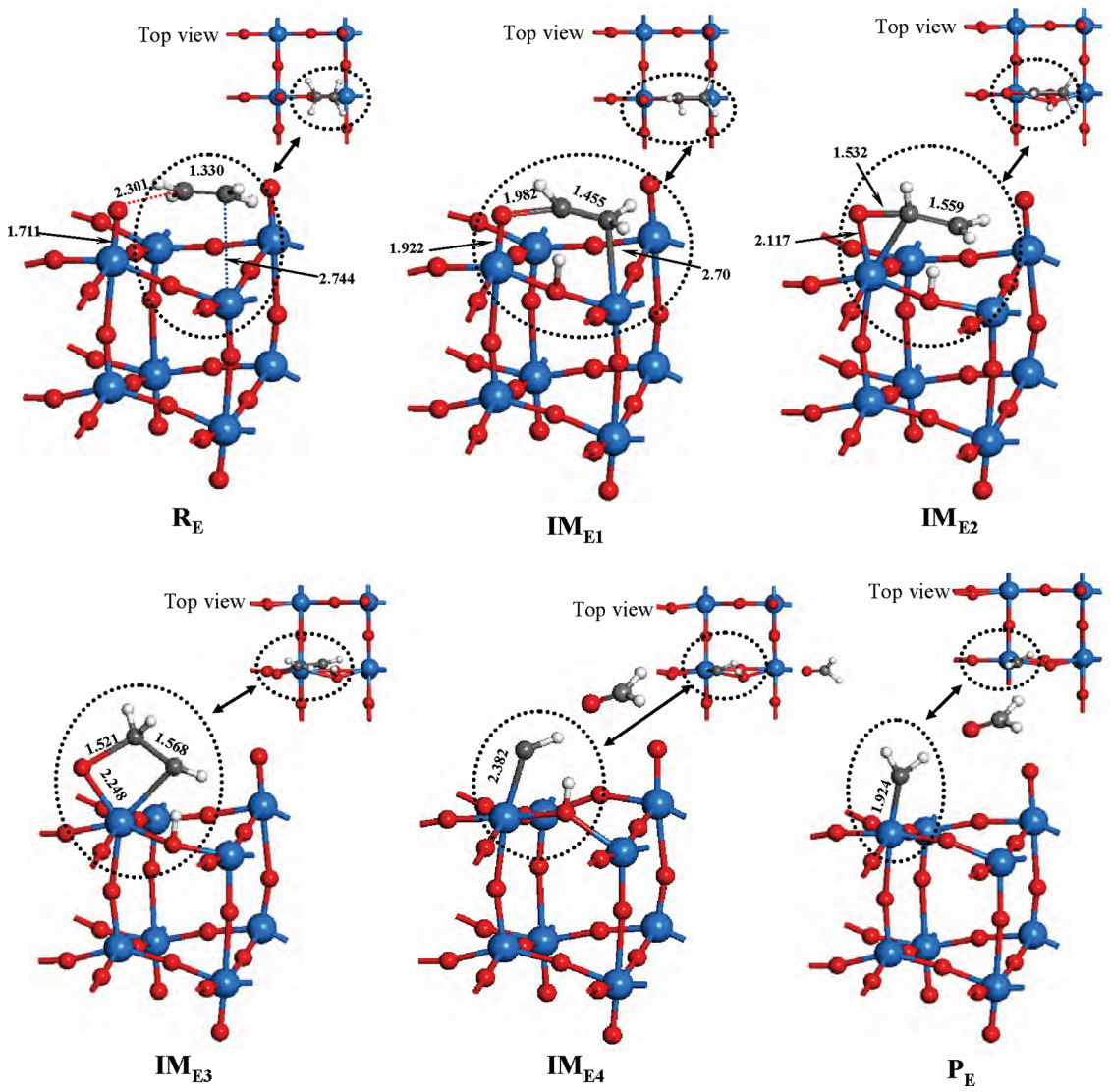

Figure 4. Optimized geometries of reactant, intermediates, and product for proposed reaction pathway to form W = CH_2 active sites via ethene activation. The bond length is in Å.

the single site absorption configuration corresponding to O_{2c}···C═C is also energetically unfavorable, because of steric repulsion with the adjacent W-oxo site. Thus, we conclude that W_{5c}···C═C···O_{1c} (R_E) is the most likely configuration for adsorbed ethene on WO_3 (001).

For 2-butene, the one site adsorption configuration corresponding to O_{1c}···C═C is the most energetically favorable, with E_{ads} = −20.35 kJ/mol. Because of steric repulsion from the large methyl groups in 2-butene, two site absorption is not favored; again, the configuration corresponding to O_{1c}···C═C···O_{1c} is the least energetically favorable. Thus, we conclude that O_{1c}···C═C (R_B) is the most likely configuration for adsorbed 2-butene on WO_3 (001).

3.3. Formation of Active Sites for Olefin Metathesis. We take the most energetically stable adsorbate configurations, W_{5c}···C═C···O_{1c} for ethene and O_{1c}···C═C for butene, as our initial state (R) for the metathesis reaction. Since the reaction pathway to form W-carbene active sites involves several intermediates, different potential oxametallacycle intermediates (IM)[58,59] were postulated by comparison of their adsorption energys, so that together they yield a five-step process (Scheme 2).

3.3.1. Active Sites for Ethene Metathesis. As shown in Figure 4, the first intermediate formed by ethene is a six-membered oxametallacycle (IM_{E1}) from the initial W_{5c}···C═C···O_{1c} reactant, R_E. The transition state, TS_{E1}, involves olefin activation via migration of hydrogen from ethene to surface-bound O_{2c}, so that a weak W_{6c}-C bond is formed. The W═O bond increases in length from 1.711 Å in R_E to 1.922 Å in In_{E1}. The C_1−C_2 bond increases in length from 1.330 Å in R_E to 1.455 Å in In_{E1}. Two new bonds, W_{5c}-C and O_{1c}-C, are formed with bond lengths of 2.70 Å and 1.982 Å, respectively. The second intermediate formed by ethene is a three membered W_{6c}−C-O ring (IM_{E2}). The transition state, TS_{E2}, involves the cleavage of the W_{5c}-C bond and the formation of a weak W_{6c}-C bond. The third intermediate formed by ethene is a four-membered oxametallacycle (IM_{E3}). It was obtained by breaking the previous weak W_{6c}-C bond and forming a new W_{6c}-C bond of 2.336 Å with the second C atom. This structure can greatly reduce ring strain. We thus see that the first three transition states, TS_{E1}, TS_{E2}, and TS_{E3}, consist of nearly flat oxametalla-

dx.doi.org/10.1021/cs2005778 | ACS Catal. 2012, 2, 341−349

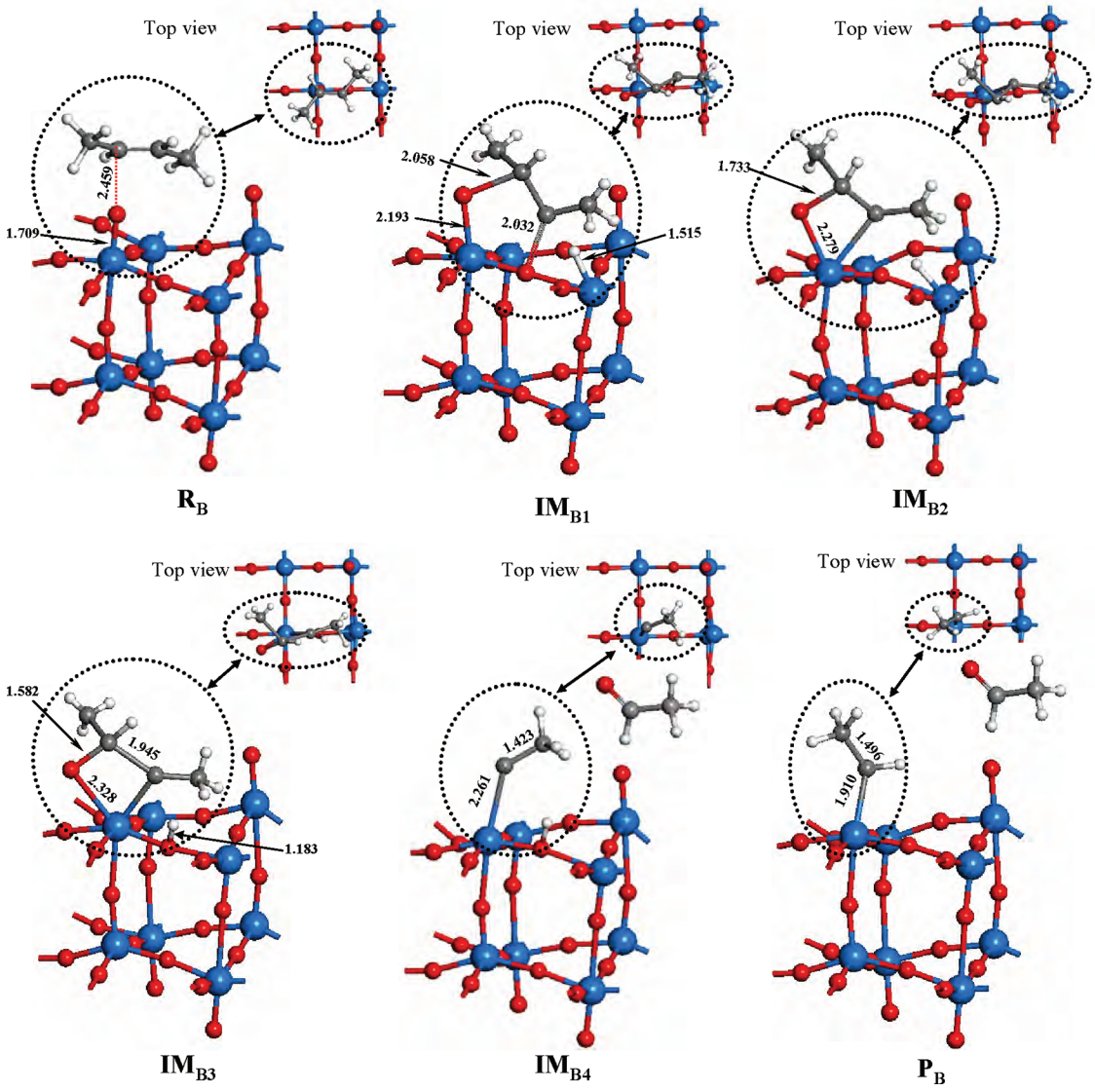

Figure 5. Optimized geometries of reactant, intermediates, and product for the proposed reaction pathway to form W = CH−CH_3 active sites via 2-butene activation. The bond length is in Å.

cycles, with dihedral angles of 163.5°, 159.7°, and 173.1°, respectively.

The fourth intermediate step involves the formation of the fourth transition state, TS_{E4}, which is the decomposition of the four-membered oxametallacycle and the lengthening of the C−C bond. Formaldehyde (H_2C=O, methanal) is evolved into the gas phase. Finally, the W_{6c}=CH group quickly undergoes hydrogen redistribution via the fifth transition state TS_{E5}, to form the final W=CH_2 active site, P_E, with a W=C bond length of 1.924 Å. The whole process is depicted in Figure 4.

3.3.2. Active Sites for 2-Butene Metathesis. The first intermediate formed by 2-butene is a five-membered oxametallacycle (IM_{B1}) from the initial O_{1c}···C=C reactant, R_B. The transition state, TS_{B1}, involves olefin activation via migration of hydrogen from 2-butene to surface-bound W_{5c}, so that a O_{2c}-C bond is formed with bond length 2.032 Å. A O_{1c}-C bond is also formed with bond length 2.058 Å. Furthermore, the bond order of W_{6c}=O_{1c} is reduced from a double bond to that of a single bond. The second intermediate formed by 2-butene is a four-membered oxametallacycle (IM_{B2}). The transition state, TS_{B2}, involves the cleavage of the O_{2c}-C bond and the formation of a W_{6c}-C bond to achieve the decomposition of the oxametallacycle. This process may be treated as a [2 + 2] cycloaddition reaction between the W_{6c}-O_{1c} and C_1−C_2 bonds to form IM_{B2} as the 2-butene moiety moves closer to W_{6c}. The third intermediate formed by 2-butene is also a four-membered oxametallacycle (IM_{B3}), but involves migration of hydrogen from W_{5c} to O_{2c}. Now, we see that IM_{B3} resembles IM_{E3}, but that the W_{6c}-C bond length is 0.351 Å longer in IM_{B3} than in IM_{E3}. The fourth intermediate step involves the formation of the fourth transition state, TS_{B4}, which is the decomposition of the four-membered oxametallacycle and the total cleavage of both the original 2-butene C=C bond and the W_{6c}-O_{1c}. Acetaldehyde (H_3C−CH=O, ethanal) is evolved into the gas phase. Finally, the W_{6c}=C−CH_3 group quickly undergoes hydrogen redistribution via the fifth transition state, TS_{B5}, to form the final W=CH−CH_3 active site, P_B, with a W=C bond length of 1.910 Å. The whole process is depicted in Figure 5

3.4. Activation Energies for Active Site Formation. The energy diagram depicting ethene reacting on WO_3 (001) to form W=CH_2 active sites is presented in Figure 6. We

dx.doi.org/10.1021/cs2005778 | *ACS Catal.* 2012, 2, 341−349

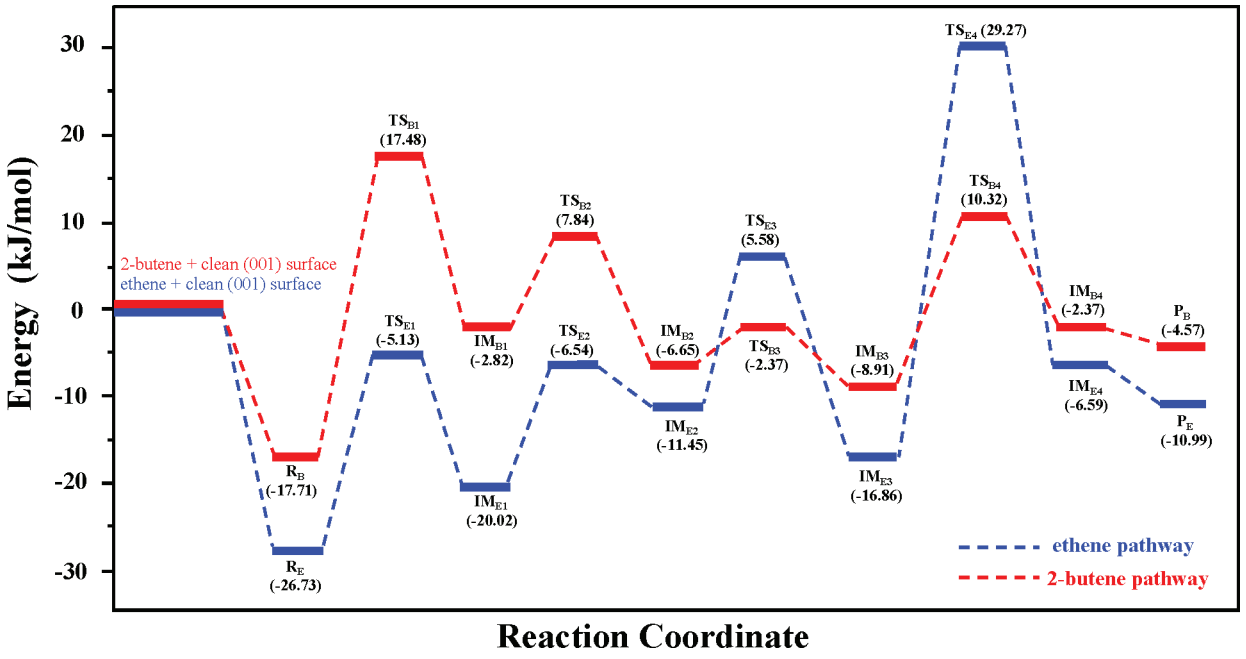

Figure 6. Minimum energy paths for ethene (blue) and 2-butene (red), with corresponding activation energies, for W-carbene active site formation on WO_3 (001).

normalize the total energy of the constituent components (e.g., gas-phase ethene and clean WO_3 (001)) to zero. From Table 1, we thus mark the energy of the reactant, R_E, to be −26.73 kJ/mol. We see that the formation of the first intermediate, IM_{E1}, from the reactant, R_E, has a computed activation energy barrier of E_a = +21.6 kJ/mol and is endothermic, with E_{ads} = +6.71 kJ/mol. The formation of the second intermediate, IM_{E2}, has E_a = +13.48 kJ/mol and is also endothermic, with E_{ads} = +8.57 kJ/mol. The formation of the third intermediate, IM_{E3}, has E_a = +17.03 kJ/mol and is the first exothermic step, with E_{ads} = −5.41 kJ/mol. We note that IM_{E3} consists of the W_{6c}···C═C···O_{1c} adsorption configuration first described in Table 1, yet IM_{E3} is 1.71 kJ/mol lower in energy than ethylene adsorbed to WO_3 (001) in the W_{6c}···C═C···O_{1c} configuration. The "hydrogen effect" stabilizes the hydrocarbon radical via hydrogen coadsorption, and this effect has also been observed previously for related reactions on oxide surfaces.[60−66] In the next step, the oxametallacycle ring is opened to form the fourth intermediate, IM_{E4}. The final hydrogen redistribution from O_{2c} to the neighboring W═CH site is barrierless, yet the overall process of forming the W-carbene active site is endothermic (ΔE = +15.74 kJ/mol). When comparing all energy barriers in the ethene pathway, it is easily seen that the oxametallacycle ring-opening has the highest activation energy barrier of E_a = +46.13 kJ/mol.

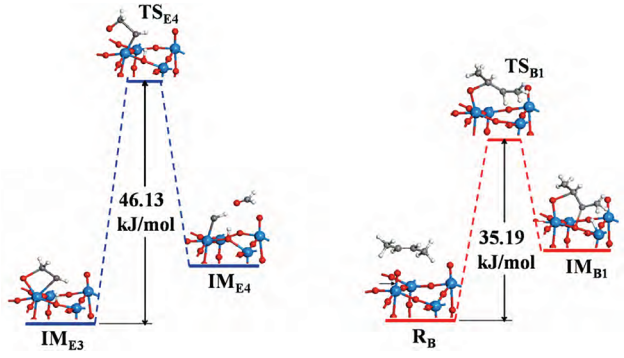

Figure 7. Transition states for rate limiting steps in ethene (left, blue) and 2-butene (right, red) pathways.

The energy diagram depicting 2-butene reacting on WO_3 (001) to form W═CH−CH_3 active sites is also presented in Figure 6. Again, we normalize the total energy of the constituent components (e.g., gas-phase 2-butene and clean WO_3 (001)) to zero. From Table 1, we thus mark the energy of the reactant, R_B, to be −17.71 kJ/mol. The formation of the first intermediate, IM_{B1}, from the reactant R_B has the highest activation energy barrier of E_a = +35.19 kJ/mol and is endothermic, where E_{ads} = +14.89 kJ/mol. The second and third intermediates form exothermically, with low activation energy barriers of E_a = +10.66 kJ/mol for TS_{B2} and E_a = +4.28 kJ/mol for TS_{B3}. The decomposition of the four-membered oxametallacycle via TS_{B4} has a relatively high E_a = +19.23 kJ/mol and is again endothermic. The final hydrogen redistribution from O_{2c} to the neighboring W═C−CH_3 site is barrierless, yet the overall process of forming the W-carbene active site is again endothermic (ΔE = +13.14 kJ/mol).

4. DISCUSSION

We have thus computed pathways for active site formation via ethene and 2-butene activation. Since both sets of metal-carbene species are formed on W_{6c}. We know that IM_{E3} and IM_{B3} are more energetically stable than their IM_{E4} and IM_{B4} counterparts in both pathways. Energy must thus be added to these intermediate configurations to cross the activation barriers. Even when hydrogen migrates to unsaturated carbons to form P_E and P_B, these final states are also higher in energy than IM_{E3} and IM_{B3}, respectively. Thus, these active sites will proceed to react with new ethene or 2-butene molecules easily and quickly in the propagation step of the metathesis process.

Also, we can see that the rate-limiting step in the ethene pathway is the cycloreversion of the four-membered

dx.doi.org/10.1021/cs2005778 | ACS Catal. 2012, 2, 341−349

oxametallacycle to release formaldehyde, with the transition state depicted in Figure 7. This four-membered ring is particularly energetically stable with little steric repulsion, so the activated hydrocarbons are strongly bound to the oxide surface. Thus, the activation energy barrier is very high (+46.13 kJ/mol). By contrast, the analogous step in the 2-butene pathway, where acetaldehyde is released, has a much lower activation energy barrier (+19.23 kJ/mol). In this pathway, the four-membered ring contains dangling methyl groups that result in unfavorable steric effects with the hydrogenated oxide surface. Thus, the ring-opening reaction is much more energetically favorable in the 2-butene pathway than in the ethene pathway.

Instead, the rate-limiting step in the 2-butene pathway is the electrophilic addition to form the oxametallacycle, with the transition state depicted in Figure 7. Although the methyl groups in 2-butene are electron-donating, thus favoring this reaction, the steric effects oppose the electrophilic effects. Thus, the activation energy barrier is very high (+35.19 kJ/mol). By contrast, the steric effects are not present in the ethene pathway, so the activation energy barrier is much lower (+21.6 kJ/mol).

In summary, the 2-butene pathway is projected to be kinetically faster than the ethene pathway to form W-carbene active sites for olefin metathesis, because of the latter's extremely high activation energy barrier to breaking the oxametallacycle intermediate. This result suggests that using a higher ratio of 2-butene to ethene will promote the formation of W-carbene active sites on WO_3 catalysts, and enhance the activity of this catalysis for olefin metathesis and propene formation.

5. CONCLUSIONS

A comprehensive DFT study of the mechanisms for forming W-carbene active sites is presented here, to lend insight into the metathesis reaction between ethene and 2-butene to form propene on WO_3 catalysts. We first show that on the most thermodynamically stable WO_3 (001) surface, four chemically distinguishable types of surface atoms are present: 5-fold coordinate W_{5c}, 6-fold coordinate W_{6c}, 2-fold bridging oxygen O_{2c}, and singly coordinated oxygen O_{1c}. Ethene adsorbs preferentially to the oxide surface in a two-site $W_{5c}\cdots C{=}C\cdots O_{1c}$ configuration, while 2-butene adsorbs preferentially in a one-site $O_{1c}\cdots C{=}C$ configuration. The reaction pathways for W-carbene active site formation differ between ethene and 2-butene, though both proceed via five-step processes. In the ethene pathway, six-membered, five-membered, and four-membered oxametallacycles are formed successively. However, in the 2-butene pathway, only five-membered and four-membered oxametallacycles are formed. We also find that the opening of the four-membered oxametallacycle is the rate-limiting step of the ethene pathway, while the forming of the five-membered oxametallacycle is the rate-limiting step of the 2-butene pathway. We ultimately find that 2-butene preferentially forms W-carbene active sites, compared to ethene, because of the presence of electrophilic and steric effects that destabilize the intermediates. These results provide us with design guidelines for propene synthesis on WO_3 catalysts.

AUTHOR INFORMATION

Corresponding Author

*E-mail: clo@wustl.edu.

Funding

This research was supported in part by the National Science Foundation through TeraGrid resources provided by the National Center for Supercomputing Applications under Grant TG-CTS110011.

ACKNOWLEDGMENTS

The authors thank the Center of Excellence on Catalysis and Catalytic Reaction Engineering at Chulalongkorn University in Thailand, particularly the groups of Suphot Phatanasri and Piyasan Praserthdam, for helpful advice and guidance on understanding the experimental basis for olefin metathesis on oxide catalysts. The authors also thank Gregory Yablonsky for helpful comments and suggestions for our manuscript.

REFERENCES

(1) Oikawa, H.; Shibata, Y.; Inazu, K.; Iwase, Y.; Murai, K.; Hyodo, S.; Kobayashi, G.; Baba, T. *Appl. Catal., A* **2006**, *312*, 181−185.
(2) Spronk, R.; Vanveen, J. A. R.; Mol, J. C. *J. Catal.* **1993**, *144*, 472−483.
(3) Mol, J. C. *Catal. Today* **1999**, *51*, 289−299.
(4) Inaki, Y.; Yoshida, H.; Kimura, K.; Inagaki, S.; Fukushima, Y.; Hattori, T. *Phys. Chem. Chem. Phys.* **2000**, *2*, 5293−5297.
(5) Mitra, B.; Gao, X.; Wachs, I. E.; Hirt, A. M.; Deo, G. *Phys. Chem. Chem. Phys.* **2001**, *3*, 1144−1152.
(6) Mol, J. C. *J. Mol. Catal. A: Chem.* **2004**, *213*, 39−45.
(7) Grubbs, R. H. *Angew. Chem., Int. Ed.* **2006**, *45*, 3760−3765.
(8) Tsuji, J. *Transition Metal Reagents and Catalysts*; John Wiley & Sons, Ltd: Chichester, U.K., 2003.
(9) Banks, R. Catalysis. In *Topics in Current Chemistry*; Springer: Berlin/Heidelberg, Germany, 1972; Vol. 25; pp 39−69.
(10) Thomas, R.; van Oers, E. M.; de Beer, V. H. J.; Moulijn, J. A. *J. Catal.* **1983**, *84*, 275−287.
(11) Ivin, K. J.; Mol, J. C. *Olefin Metathesis and Metathesis Polymerization*; Academic Press: San Diego, 1997.
(12) Davazoglou, D.; Moutsakis, A.; Valamontes, V.; Psycharis, V.; Tsamakis, D. *J. Electrochem. Soc.* **1997**, *144*, 595−599.
(13) Huang, S.; Liu, S.; Xin, W.; Bai, J.; Xie, S.; Wang, Q.; Xu, L. *J. Mol. Catal A: Chem.* **2005**, *226*, 61−68.
(14) Huang, S.; Liu, S.; Zhu, Q.; Zhu, X.; Xin, W.; Liu, H.; Feng, Z.; Li, C.; Xie, S.; Wang, Q.; Xu, L. *Appl. Catal., A* **2007**, *323*, 94−103.
(15) Liu, H.; Huang, S.; Zhang, L.; Liu, S.; Xin, W.; Xu, L. *Catal. Commun.* **2009**, *10*, 544−548.
(16) Chaemchuen, S.; Phatanasri, S.; Verpoort, F.; Sae-ma, N.; Suriye, K. *Kinet. Catal.*, in press.
(17) Jean-Louis Hérisson, P.; Chauvin, Y. *Makromol. Chem.* **1971**, *141*, 161−176.
(18) Shelimov, B. N.; Elev, I. V.; Kazansky, V. B. *J. Mol. Catal.* **1988**, *46*, 187−200.
(19) Tarasov, A. L.; Shelimov, B. N.; Kazansky, V. B.; Mol, J. C. *J. Mol. Catal. A: Chem.* **1997**, *115*, 219−228.
(20) Adlhart, C.; Chen, P. *Angew. Chem., Int. Ed.* **2002**, *41*, 4484−4487.
(21) Wu, Y.-D.; Peng, Z.-H. *Inorg. Chim. Acta* **2003**, *345*, 241−254.
(22) Goumans, T. P. M; Ehlers, A. W.; Lammertsma, K. *Organometallics* **2005**, *24*, 3200−3206.
(23) Handzlik, J.; Ogonowski, J.; Tokarz-Sobieraj, R. *Catal. Today* **2005**, *101*, 163−173.
(24) Handzlik, J. *Surf. Sci.* **2007**, *601*, 2054−2065.
(25) Adlhart, C.; Chen, P. *J. Am. Chem. Soc.* **2004**, *126*, 3496−3510.
(26) Grubbs, R. H. *Tetrahedron* **2004**, *60*, 7117−7140.
(27) Schrock, R. R. *J. Mol. Catal. A: Chem.* **2004**, *213*, 21−30.
(28) Handzlik, J.; Sautet, P. *J. Catal.* **2008**, *256*, 1−14.
(29) Handzlik, J.; Ogonowski, J. *Catal. Lett.* **2003**, *88*, 119−122.
(30) Wu, Y.-D.; Peng, Z.-H. *J. Am. Chem. Soc.* **1997**, *119*, 8043−8049.
(31) Cavallo, L. *J. Am. Chem. Soc.* **2002**, *124*, 8965−8973.

(32) Vyboishchikov, S. F.; Bühl, M.; Thiel, W. *Chem.—Eur. J.* **2002**, *8*, 3962−3975.
(33) Sastre, G. *Phys. Chem. Chem. Phys.* **2007**, *9*, 1052−1058.
(34) Boronat, M.; Concepcion, P.; Corma, A.; Navarro, M. T.; Renz, M.; Valencia, S. *Phys. Chem. Chem. Phys.* **2009**, *11*, 2876−2884.
(35) Sundberg, M.; Tilley, R. J. D. *J. Solid State Chem.* **1974**, *11*, 150−160.
(36) Salje, E.; Carley, A. F.; Roberts, M. W. *J. Solid State Chem.* **1979**, *29*, 237−251.
(37) Tanisaki, S. *J. Phys. Soc. Jpn.* **1960**, *15*, 566−573.
(38) Salje, E.; Viswanathan, K. *Acta Crystallogr.* **1975**, *A31*, 356−359.
(39) Wijs, G. A. d.; Boer, P. K. d.; Groot, R. A. d.; Kresse, G. *Phys. Rev. B* **1999**, *59*, 2684−2693.
(40) Migas, D. B.; Shaposhnikov, V. L.; Rodin, V. N.; Borisenko, V. E. *J. Appl. Phys.* **2010**, *108*, 093713.
(41) Ling, S.; Mei, D.; Gutowski, M. *Catal. Today* **2011**, *165*, 41−48.
(42) Salje, E. *Acta Crystallogr.* **1977**, *B33*, 574−577.
(43) Woodward, P.; Sleight, A.; Vogt, T. *J. Solid State Chem.* **1997**, *131*, 9−17.
(44) Roussel, P.; Labbé, P.; Leligny, H.; Groult, D.; Foury-Leylekian, P.; Pouget, J. P. *Phys. Rev. B* **2000**, *62*, 176−188.
(45) Dixon, R.; Williams, J.; Morris, D.; Rebane, J.; Jones, F.; Egdell, R.; Downes, S. *Surf. Sci.* **1998**, *399*, 199−211.
(46) Tanner, R. E.; Meethunkij, P.; Altman, E. I. *J. Phys. Chem. B* **2000**, *104*, 12315−12323.
(47) Tanner, R. E.; Altman, E. I. *J. Vac. Sci. Technol., A* **2001**, *19*, 1502−1509.
(48) Jones, F.; Rawlings, K.; Foord, J.; Egdell, R.; Pethica, J.; Wanklyn, B.; Parker, S.; Oliver, P. *Surf. Sci.* **1996**, *359*, 107−121.
(49) Ma, S.; Frederick, B. G. *J. Phys. Chem. B* **2003**, *107*, 11960−11969.
(50) Kresse, G.; Hafner, J. *Phys. Rev. B* **1993**, *47*, 558−561.
(51) Kresse, G.; Furthmüller, J. *Comput. Mater. Sci.* **1996**, *6*, 15−50.
(52) Kresse, G.; Furthmüller, J. *Phys. Rev. B* **1996**, *54*, 11169−11186.
(53) Perdew, J. P.; Burke, K.; Ernzerhof, M. *Phys. Rev. Lett.* **1996**, *77*, 3865−3868.
(54) Blöchl, P. E. *Phys. Rev. B* **1994**, *50*, 17953−17979.
(55) Kresse, G.; Joubert, D. *Phys. Rev. B* **1999**, *59*, 1758.
(56) Yakovkin, I.; Gutowski, M. *Surf. Sci.* **2007**, *601*, 1481−1488.
(57) Jónsson, H.; Mills, G.; Jacobsen, K. W. In *Classical and Quantum Dynamics in Condensed Phase Simulations*; Berne, B. J., Ciccotti, G., Coker, D. F., Eds.; World Scientific: Singapore, 1998; pp 385−404.
(58) Medlin, J.; Barteau, M. A.; Vohs, J. M. *J. Mol. Catal A: Chem.* **2000**, *163*, 129−145.
(59) Linic, S.; Barteau, M. A. *J. Am. Chem. Soc.* **2002**, *124*, 310−317.
(60) Paál, Z., Menon, P. G., Eds. *Hydrogen effects in catalysis: fundamentals and practical applications*; M. Dekker: New York, 1988.
(61) Onda, K.; Li, B.; Zhao, J.; Jordan, K. D.; Yang, J.; Petek, H. *Science* **2005**, *308*, 1154−1158.
(62) Sushko, M. L.; Gal, A. Y.; Shluger, A. L. *J. Phys. Chem. B* **2006**, *110*, 4853−4862.
(63) Zhao, J.; Li, B.; Jordan, K. D.; Yang, J.; Petek, H. *Phys. Rev. B* **2006**, *73*, 195309.
(64) Raghunath, P.; Lin, M. C. *J. Phys. Chem. C* **2008**, *112*, 8276−8287.
(65) Chang, C. Y.; Chen, H.-T.; Lin, M. C. *J. Phys. Chem. C* **2009**, *113*, 6140−6149.
(66) Huang, W.-F.; Chen, H.-T.; Lin, M. C. *J. Phys. Chem. C* **2009**, *113*, 20411−20420.